05,10,16

Magnetoopticalal effects in $Zn_{1-x}Co_xFe_2O_4$ and $Mg_{1-x}Co_xFe_2O_4$ mixed ferrite nanoparticles

© A.E. Sokolov[1,2], I.S. Edelman[1], O.S. Ivanova[1,2], R.D. Ivantsov[1], D.A. Petrov[1], Yu.V. Knyazev[1,2], A. Thakur[3], P. Thakur[3]

[1] Kirensky Institute of Physics, Federal Research Center KSC SB, Russian Academy of Sciences, Krasnoyarsk, Russia
[2] Siberian Federal University, Krasnoyarsk, Russia
[3] Amity University Haryana, Gurugram, Haryana, India

E-mail: osi@iph.krasn.ru

Received July 14, 2025
Revised July 16, 2025
Accepted July 17, 2025

Mixed Zn-Co and Mg-Co ferrite nanoparticles (NPs) with the formulas $Zn_{1-x}Co_xFe_2O_4$ and $Mg_{1-x}Co_xFe_2O_4$ where x was equal to 0.0, 0.2, and 0.4 were synthesized via auto- combustion method using citrate precursor as a catalyst that initiates a thermal reaction. X-ray diffraction patterns showed that for all compositions, NPs are nanocrystals of the Fd-3m space group. ^{57}Fe Mössbauer spectroscopy showed all Co^{2+} ions in Mg-Co ferrite to occupy the octahedral positions only and Fe^{3+} ions to be distributed approximately equally between octahedral and tetrahedral positions. In Zn-Co ferrite NPs, Co^{2+} ions are distributed approximately evenly between these interstitial positions, and Fe^{3+} ions are localized preferably in octahedral positions. Magnetic measurements demonstrate large values of saturation magnetization, M_s, in both cases but high coercivity, H_c, in the first case and low coercivity in the second one. Spectra of the Faraday effect and magnetic circular dichroism were obtained for such mixed ferrites for the first time and their dependence on the nature of the non-magnetic ion and cobalt concentration was analyzed. In particular, the analysis carried out allowed us to associate unambiguously the strong peak in the near infrared region with the spin allowed crystal field electron transition in Co^{2+} ions situated in octahedral positions

Keywords: nanostructure, magnetic properties, Mössbauer effect, magnetic circular dichroism, Faraday effect.

DOI: 10.61011/PSS.2025.08.62264.194-25

1. Introduction

The magnetooptical effects due to interaction of electromagnetic radiation with matter played an important role in the early history of electromagnetism and now they are still one of the important tools in matter research [1–7]. In modern engineering, the magnetooptical effects are extremely widely applied: from magnetooptical sensors [8] and light beam controllers [9] to laser interferometry when studying gravitational waves [10]. The magnetooptical effects in ferrite spinels are studied for quite a long time. It mainly includes investigation of Kerr effects in reflected light on crystals and films and analysis of spectral dependences of an off-diagonal component of the dielectric tensor ε''_{xy} [11–18]. The literature results and especially their interpretation by various authors significantly differ. It is attributed to complex distribution of metal cations between crystal positions in a spinel structure and, in many cased, to presence of multivalent cations. Thus, it is still relevant to find out a nature of the magnetooptical effects in the ferrite spinels, which is not only of a fundamental interest, but it is also necessary for applied use of specific compounds.

The main type of magnetic-ordered materials used for creating magnetooptical devices is ferrite garnets [19–21], which demonstrate high magnetooptical activity in the visible and near-ultraviolet (UV) spectral ranges [19]. The cobalt-containing ferrite spinels are characterized by an intense peak in the spectrum of magnetic circular dichroism (MCD) in the near-infrared (IR) range [22], which is centered at 1.75 eV. It corresponds to a radiation wavelength (710 nm) of some solid-state lasers (for example, ALP-710 nm, NKT Photonics, Denmark) and diodes, which are produced by many companies (for example, BMI SURPLUS Inc., USA). It may be interesting for designing near-IR range photonics devices. From this point of view, a material to be used in specific devices shall have not only quite high magnetooptical activity, but certain magnetic properties as well, for example, a small or large coercive force for operation at various frequency modes.

The present study is dedicated to investigating the magnetooptical properties of nanoscale crystals of the families $Zn_{1-x}Co_xFe_2O_4$ and $Mg_{1-x}Co_xFe_2O_4$ in a dependence of distribution of the magnetic cations between the crystal position, which is obtained using the Mössbauer effect. In these families, extreme members of the ZnF_2O_4 series are a normal spinel, in which the Zn^{2+} ions occupy tetrahedral (A) positions, while the Fe^{3+} occupy octahedral (B) positions; while in MgF_2O_4 the ions Mg^{2+} and Fe^{3+}

occupy both types of the positions. CoF_2O_4 has a structure of the partly inverted spinel, where the ions Fe^{3+} and Co^{2+} occupy both the A- and B-positions with an inversion parameter from 0.6 to 0.9 [23,24]. A variety of ion distributions can be observed in the real situation, which are determined by many factors. First of all, it is a ratio between ion radii and radii of the voids between the oxygen ions. Thus, the ion radii $r(Fe^{3+}) = 0.64$ Å, $r(Co^{2+}) = 0.74$ Å, $r(Mg^{2+}) = 0.72$ Å, $r(Zn^{2+}) = 0.74$ Å; while the voids radii in the MgF_2O_4 structure is 0.72 Å for octahedrons and 0.58 Å for tetrahedron; in the ZnF_2O_4 structure is 0.7 Å for octahedrons and 0.65 Å for tetrahedrons. An electron configuration of the ion is of high importance: for example, the Zn^{2+} ions tend to occupy tetrahedral sites so that their 4sp-electrons could form a covalent bond with 2p-electrons of oxygen. Taking into account the Madelung electrostatic energy leads to the fact that an energetically favorable state can be a state when the ions with the least positive charge enter the neighborhood with 4 oxygen ions, while the ions with the highest positive charge enter the neighborhood with 6 oxygen ions despite the ratio of the radii of the ion and the voids. These and some other factors result in that in the reality both the bivalent and the trivalent ions can occupy the A- and B-positions. In case of nanocrystals, the task is complicated due to their size distribution, disordered surface layers, the influence of an effective media, in which they are, interparticle interaction, etc. The synthesis method crucially affects all these factors and, therefore, position distribution of the ions and, therefore, the magnetic and magnetooptical properties of samples. The nanocrystals were synthesized by an auto- combustion method using a citrate precursor as a thermal reaction catalyst. In case of the nanocrystals, it is believed that the most informative study is a study of effects in transmitted light — the Faraday effect (FE) and MCD. At the same time, MCD is the most convenient for interpretation, since it is observed only in ranges of the absorption bands of the studied samples.

2. Samples and measurement procedure

The nanoparticles $Zn_{1-x}Co_xFe_2O_4$ and $Mg_{1-x}Co_xFe_2O_4$ with $x = 0, 0.2$ and 0.4 were synthesized by the auto- combustion method using the citrate precursor as the thermal reaction catalyst. In the first case, the initial components were zinc nitrate hexa-hydrate ($Zn(NO_3)_2 \cdot 6H_2O$), cobalt nitrate hexa-hydrate ($Co(NO_3)_2 \cdot 6H_2O$) and iron(III) nitrate nona-hydrate ($Fe(NO_3)_3 \cdot 9H_2O$), which were dissolved in 125 ml of distilled water. In the second case, magnesium nitrate hexa-hydrate ($Mg(NO_3)_2 \cdot 6H_2O$) was used instead of Zn nitrate hexa-hydrate. 5 g of citric acid was added into a produced mixture and mixed at 80 °C in order to produce a homogeneous solution. The solution was held at 80 ± 5 °C until water was fully evaporated to produce a brown gel. It is followed by an auto-heating reaction with releasing a red-brown nitrogen dioxide gas, which results in formation of a black sticked powder to be later ground in an agate mortar using a pestle. The ground powder was heated to 700 °C in a muffle furnace for 3 h and then cooled naturally to the room temperature and ground again. Thus, the same technology for nanoparticle manufacturing was used in both the cases.

The crystal structure of the nanoparticles was determined by data of powder diffraction using a Bruker D8 ADVANCE powder diffractometer (Cu$K\alpha$-radiation) and a VANTEC linear detector. The increment of 2Θ was 0.02°, while the count time was 2 s per increment. The Rietveld refinement was carried out using the TOPAS 4.2 software [25]. The refinements were stable and gave low R-factors. The ^{57}Fe Mössbauer effect spectra were obtained in a MS-1104Em spectrometer in a transmission geometry with a radioactive source Co^{57}(Rh) at 300 and 4.2 K. Dependences of NP magnetization on the external magnetic field were recorded by means of a vibration magnetometer VSM 8604 (LakeShore Cryotronics) within the temperature range from 300 to 80 K in the magnetic fields up to 15 kOe.

The magnetooptical effects in transmitted light (MCD and FE) were measured using specially prepared samples: transparent plane-parallel plates, between which a NP mixture with an optically-transparent silicon-based glue was fixed (Rayher, the article № 3338100) in a weight ratio 0.5:100. The plates were placed in a laboratory-made measurement device [26] perpendicular to directions of propagation of a light beam and a vector of the external magnetic field. MCD was measured as a difference of absorbance ($\Delta D = D^+ - D^-$) of the samples for the light waves that are circularly polarized to the right (D^+) and to the left (D^-) relative to the direction of the magnetic field in the spectral range 1.2−3.8 eV in the magnetic field up to 1.3 T at 300 and 80 K. The measurement accuracy was about 10^{-4}, while spectral resolution was 20−50 cm^{-1} depending on the wavelength. The FE was measured as a rotation of an analyzer, which compensated variation of intensity of a light flux passed through the sample during its remagnetization. The FE measurement accuracy was 0.1′.

3. Results and discussion

3.1. Structure

X-ray diffraction patterns were previously studied for all the samples [27,28]. It was found that the nanoparticles have a structure of cubic spinel of a space group *Fd-3m*. In case of $Zn_{1-x}Co_xFe_2O_4$ the average crystallite size estimated by the Scherrer formula was 29−36 nm, while the lattice constant decreased from 8.443 to 8.412 Å as the concentration increase of cobalt substituting the Zn^{2+} ions. The radii of Zn^{2+} and Co^{2+} in the tetrahedral neighborhood are 0.74 and 0.72 Å respectively. Reduction of the lattice constant in this case may indicate that the Co^{2+} ions at least partially enter the tetrahedral positions. In case of $Mg_{1-x}Co_xFe_2O_4$ the average crystallite size was similar for all the compositions and it was 56 ± 3 nm. The lattice constant increased linearly from 8.387 to 8.3899 Å, which is

obviously due to a larger radius of the Co^{2+} ions (0.745 Å) in the octahedral position as compared to Mg^{2+} with the radius of 0.72 Å, i. e. with entry of Co^{2+} exactly into these positions.

3.2. Mössbauer effect

The Mössbauer effect spectra recorded at 300 and 4.2 K are shown in Figure1. In case of $Zn_{1-x}Co_xFe_2O_4$, when $T = 300$ K, quadrupole doublets (Figure1, *a*) prevail in the spectra, thereby indicating a predominantly paramagnetic state of the nanoparticles in these samples. Reduction of the measurement temperature results in essential changes in the spectra: at 4.2 K there are well-resolved sextets that are typical for the magnetic-ordered state (Figure 1, *b*); a central doublet completely disappears. These sextets are used for estimating ion distribution between the crystal positions (see Table).

The quite wide widths of doublet lines and sextet peaks are due to overlapping of several components that originate from nonequivalent states of the iron ions. Possible nonequivalent iron positions in the samples were determined by calculating distributions of probabilities of magnetic hyperfine fields. As a result, a preliminary mode spectrum was formed, whose parameters were fit into an experimental spectrum by varying the entire set of hyperfine parameters using linear approximation of the least-square method. It is clear from Table that the Co^{2+} ions enter both the tetrahedral and octahedral positions with a slight majority of the octahedrons. It agrees with the changes of the lattice parameter as per X-ray diffraction data. Note that unlike a classic situation of the normal spinel a part of the zinc ions is localized here in the octahedrons and a part of the Fe^{3+} ions is displaced into the tetrahedral positions, thereby ensuring exchange interaction of sufficient intensity for origination of the magnetic order at the low temperature.

The different situation takes place in case of $Mg_{1-x}Co_xFe_2O_4$, the well-resolved sextets are observed in the Mössbauer spectra already at the room temperature (Figure 1, *c*), and their processing similar to the previous case showed that the cobalt ions entered the octahedrons only (see Table). It also agrees with the increase of the lattice constant as per the X-ray diffraction data. It should be noted that our situation differs from results of most studies for $Mg_{1-x}Co_xFe_2O_4$, in which distribution of the Co^{2+} ions was observed among both the types of the positions [29–31]. Thus, there is a fundamental difference between distributions of the magnetic ions among the crystal positions, which shall affect the magnetic and magnetooptical properties of these two sets of the nanoparticles.

3.3. Magnetization

As noted above, the ion distribution significantly predetermined the magnetic properties of the samples, which are illustrated in Figure 2. According to predominant arrangement of the Fe^{3+} ions in one of the sublattices, the ZnF_2O_4

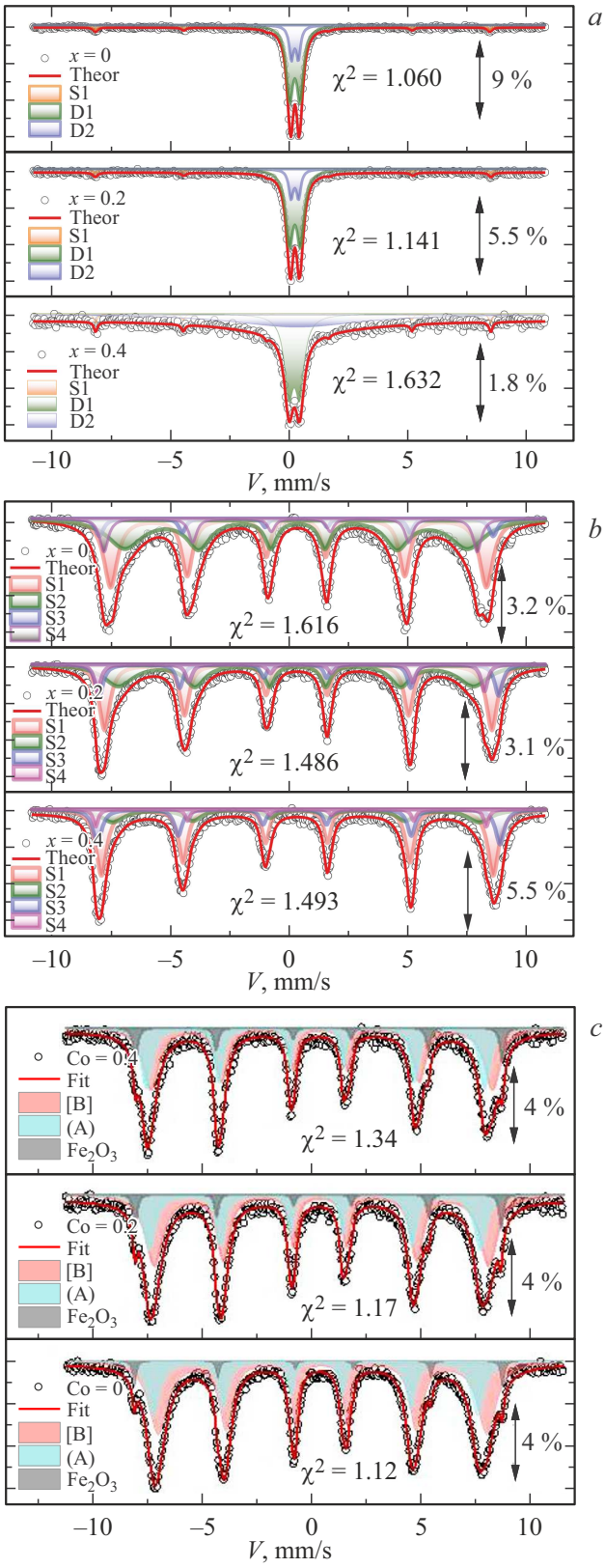

Figure 1. Mössbauer effect spectra of the nanoparticles $Zn_{1-x}Co_xFe_2O_4$ at 300 and 4.2 K (*a*, *b*) and $Mg_{1-x}Co_xFe_2O_4$ at 300 K (*c*).

Data of Mössbauer effect spectroscopy. Ion distribution between the positions.
The parentheses include the tetrahedral positions, while the square brackets include the octahedral positions

$x = 0$	$(Fe_{0.24}Zn_{0.76})\ [Fe_{1.76}Zn_{0.24}]O_4$	$(Fe_{0.95}Mg_{0.05})\ [Fe_{1.05}Mg_{0.95}]O_4$
$x = 0.2$	$(Fe_{0.12}Zn_{0.80}Co_{0.08})\ [Fe_{1.88}Co_{0.12}]O_4$	$(Fe_{0.93}Mg_{0.07})\ [Fe_{1.07}Mg_{0.73}Co_{0.2}]O_4$
$x = 0.4$	$(Fe_{0.26}Zn_{0.60}Co_{0.24})\ [Fe_{1.74}Co_{0.26}]O_4$	$(Fe_{0.94}Mg_{0.06})\ [Fe_{1.06}Mg_{0.54}Co_{0.4}]O_4$

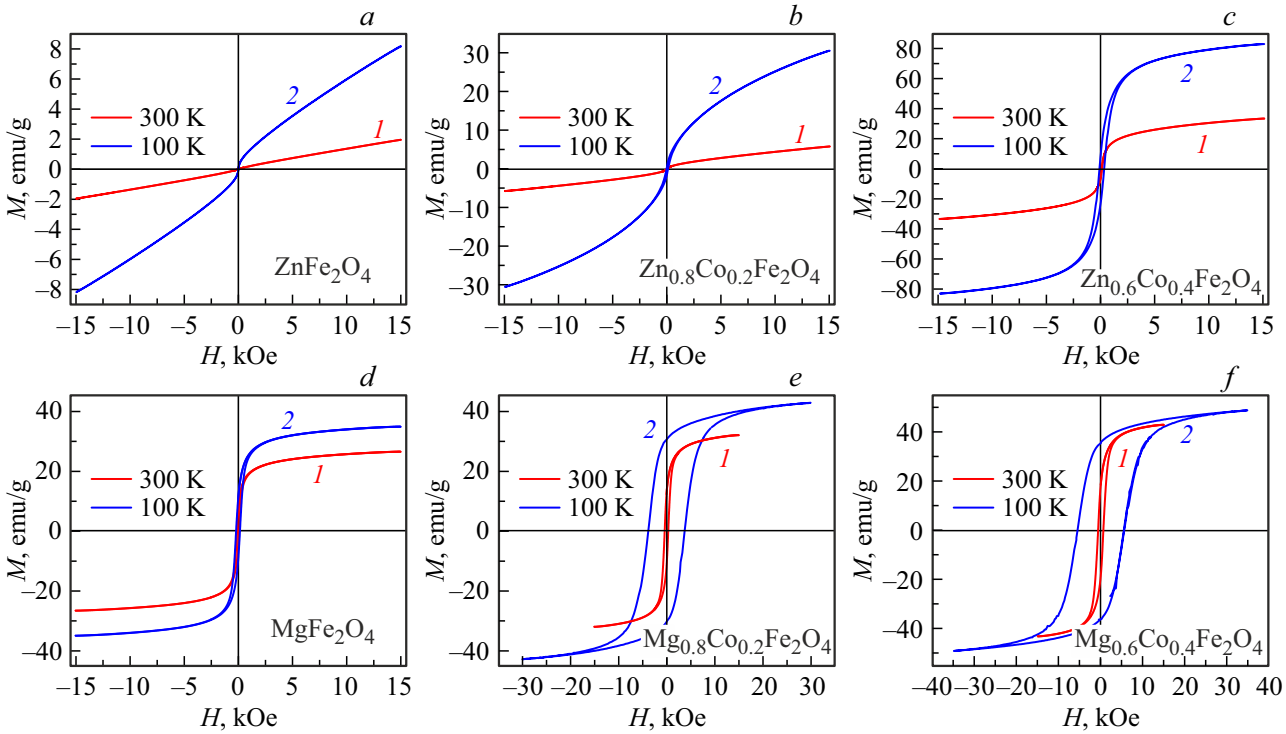

Figure 2. Field dependences of magnetization of the samples when $T = 300$ and 100 K.

samples at 300 K is paramagnetic (Figure 2, *a*, the curve *1*). However, at 100 K the magnetization curves (Figure 2, *a*, the curve *2*) exhibit a noticeable bend within the area of small fields, which indicates arising of the magnetic order. With incorporation of Co^{2+}, the magnetization curves exhibit a bend and at 100 K hysteresis with a very small coercive force becomes noticeable (Figure 2, *b* and *c*).

For MgF_2O_4, at $T = 300$ K the magnetization curves are characterized by saturation and significant hysteresis (Figure 2, *d*, which is typical for the ferrimagnetic state, and with further incorporation of cobalt or reduction of the temperature saturation magnetization and the coercive force sharply increase (Figure 2, *e* and *f*). At the same time, the concentration dependence of magnetization corresponds to this dependence calculated by the difference of the magnetic moments of the sublattices, which is determined by means of the Mössbauer effect data. With the concentration of the Co^{2+} ions, which corresponds to $x = 0.4$, saturation magnetization at the room temperature achieves a value that is sufficient for many applications, ~ 20 emu/g and 40 emu/g for Zn- and Mg-ferrites, respectively. At the same time, the coercive force H_c is 20 Oe in the first case and $H_c = 620$ Oe in the second case, at the room temperature.

3.4. Magnetooptical effects

The MCD spectra for the $Zn_{1-x}Co_xFe_2O_4$ samples are shown in Figure 3. At the room temperature, a signal of the MCD of sample not containing cobalt is at a noise level and it insignificantly exceeds it at 100 K. Since this sample has no cobalt ions, the extremely weak positive signal can be related to the Fe^{3+} ions only. With incorporation of cobalt, the signal-to-noise ratio in this area increases, a spectrum shape is gradually changed and there is a negative peak that is centered at 1.75 eV and has the signal-to-noise ratio ~ 25 at 300 K. In case of magnesium ferrite, the intense signals and the well-resolved spectra both of FE and MCD are observed already at the room temperature (Figure 4, *a*). The main specific feature are focused at the light-wave energies above 2.5 eV, which is typical for electronic transition in the Fe^{3+} ions. Unlike zinc ferrite, the spectrum shape and the effect sign do not change with reduction of the measurement temperature; only a signal intensity increases, as shown in Figure 4, *a*. With incorporation of cobalt, the shape of the spectra is changed and there is an intense negative peak that is centered near 1.75 eV in the same was as it is observed in case of Zn ferrite.

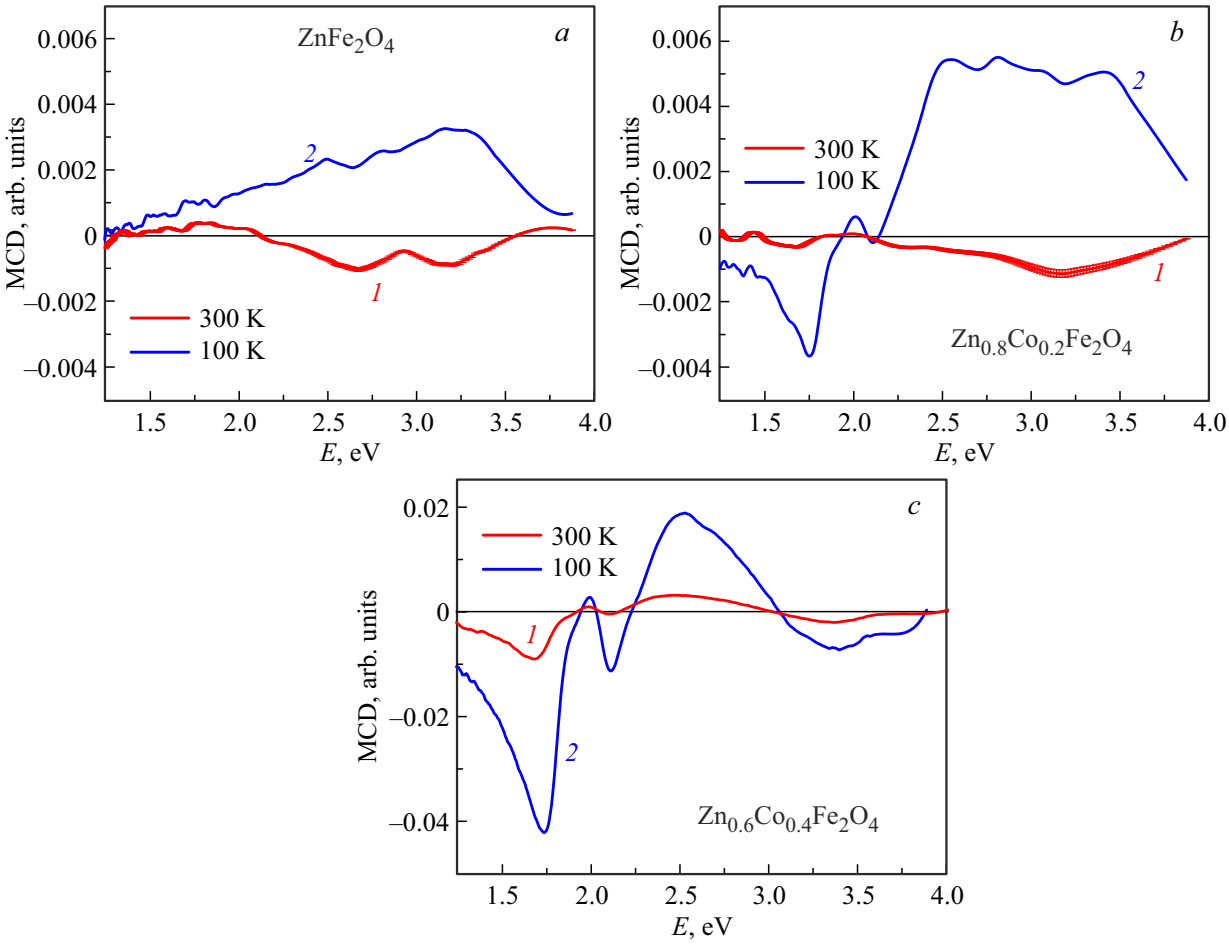

Figure 3. MCD spectra of the $Zn_{1-x}Co_xFe_2O_4$ samples at 300 and 100 K.

Let us compare the obtained MCD spectra (θ_F) with the spectra of the polar Kerr effect (θ_{K_p}) and the equatorial Kerr effect (EKE) (θ_{K_t}), which are described by similar equations [5,32]

$$\theta_F = \frac{4\pi}{\lambda}\left\{\frac{n}{k^2+n^2}\varepsilon''_{xy} - \frac{k}{k^2+n^2}\varepsilon'_{xy}\right\}, \quad (1)$$

$$\theta_{K_p} = \frac{B}{B^2-A^2}\varepsilon''_{xy} - \frac{A}{B^2-A^2}\varepsilon'_{xy}, \quad (2)$$

$$\theta_{K_t} = a(n,k,\varphi)\varepsilon'_{xy} + b(n,k,\varphi)\varepsilon''_{xy}. \quad (3)$$

Here, ε'_{xy} and ε''_{xy} are real and imaginary parts of the off-diagonal component of the permittivity tensor ε, n and k are refractive index and absorption index, a, b. A and B are combinations of diagonal components of the tensor ε and an angle of light incidence on the sample φ (in case of EKE). The ZnF_2O_4 nanoparticles contain only one type of the magnetic ions. As mentioned above, the only magnetic Fe^{3+} ions occupy the octahedral positions in the bulk samples and superexchange interaction between them provides antiferromagnetic ordering when $T < 10$ K. However, in case of the nanoparticles the part of the Fe^{3+} ions is localized in the tetrahedral positions (see Table), which, when taking into account the small size of the nanoparticles, can result in magnetic ordering at the low temperature similar to the study [33]. It is indicated by an inflection of the magnetization curve at 100 K (Figure 2, *a*). When incorporating cobalt instead of iron, the total number of the magnetic ions in both the types of the positions is insignificantly changed, but the MCD signal within the region of the energies 2–4 eV while being weak and negative at the room temperature, sharply increases during cooling of the sample (Figure 3, *b*), so does magnetization (Figure 2, *b*), and changes its sign. The Co^{2+} ions partially occupy the tetrahedral positions instead of the nonmagnetic Zn^{2+} ions and the magnetic Fe^{3+}, as it follows from the Mössbauer data. It can be assumed that due to a much larger radius of the Co^{2+} ions as compared to the Fe^{3+} ions binding angles are changed and exchange interaction increases to result in an increase of the magnetic ordering temperature and, therefore, an increase of magnetization and the magnetooptical signal at 100 K. Along with the change of the MCD sign during the temperature decrease and with a sharp increase of an absolute value of the signal at the same time, the region 2–4 eV exhibits the intense negative MCD peak centered at 1.75 eV and a S-shaped

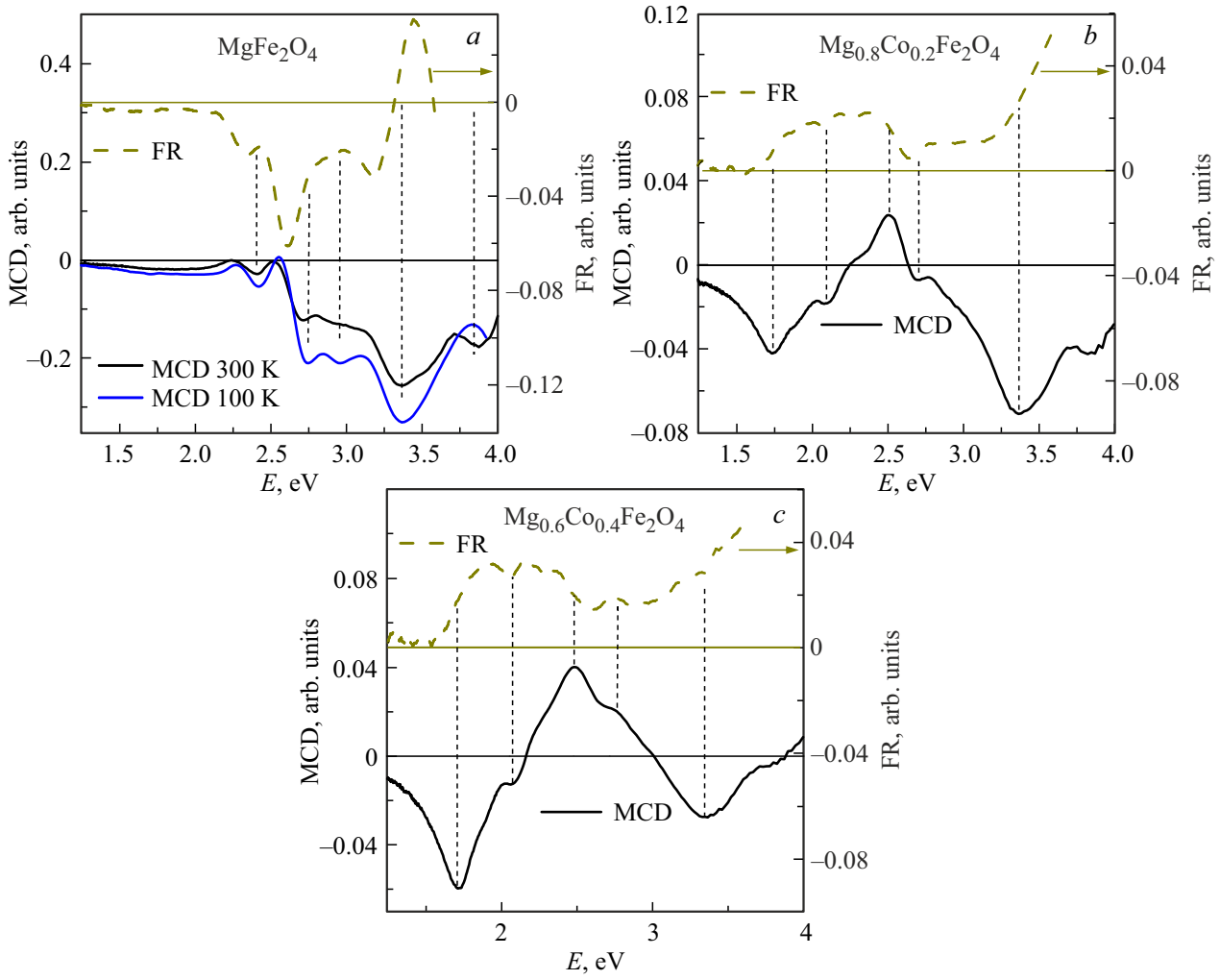

Figure 4. Spectral dependences of MCD and FE at $T = 300$ K, $H = 3.5$ kOe for the $Mg_{1-x}Co_xFe_2O_4$ samples for $x = 0, 0.2, 0.4$ — the panels *a, b, c*, respectively. *a* — the MCD spectra of the sample at $x = 0$ at 100 and 300 K.

specific feature near 2.1 eV, which are obviously related to transitions in the cobalt ions. With the increase of the Co concentration, the shape of these specific features is not changes, but the signal intensity increases (Figure 3, *c*). The high-energy part of the spectrum also has changes: instead of the set of the overlapping peaks of the same sign a positive asymmetric peak centered near 2.7 eV is left, MCD passes through zero at 3.1 eV and opposite-sign specific features appear at the high light-wave energies. These changes are obviously related to excitation of the Co^{2+} ions.

In case of the MgF_2O_4 nanoparticles the intense MCD signal is observed already at the room temperature and the spectrum is represented by a set of the negative-sign peak of various intensity (Figure 4, *a*). It almost completely coincides with the EKE spectrum provided in the study [15]. When the sample is cooled, the effect sign is not changed (Figure 4, *a*), and unlike the situation of zinc ferrite, only the absolute value of the effect increases in proportion to the increase of magnetization (Figure 2, *a*). The well-resolved FE spectrum is also observed. The gravity centers of the peaks in the MCD spectrum correspond to inflection points in the curves of the FE dependence on the light-wave energy. In case of an isolated electronic transition the positions of the MCD extremums shall correspond to the FE transition through zero [2]. Due to the S-shaped form of the FE curves and their overlapping in case of the electronic transitions that occur at close light-wave energies, there can be deviations from this rule. In particular, the FE dispersion curves in the visible range can be imposed on a „tail“ of the FE dispersion curve of the intense transition into UV, which is similar to a shift of the zero line during measurement. This situation takes place in our case. When incorporating cobalt, the spectrum shape is changed (Figure 4, *b*), which is in principle similar to the changes of the spectra of $Zn_{1-x}Co_xFe_2O_4$. At both the used Co concentrations, there are a positive and a negative peak near 2.5 and 3.4 eV, respectively. The intensity of the former increases and the intensity of the latter decreases with the increase of the Co concentration. Completely identical to the $Zn_{1-x}Co_xFe_2O_4$ nanoparticles, the negative peak appears at 1.75 eV and

its intensity increases as the Co concentration increases. Besides, there is a specific feature that is forming near 2 eV and similar to the specific feature observed at the same energy in the zinc ferrite spectrum (Figure 3, *b* and *c*), but it is much less intense.

The MCD spectra represented by the curves *2* in Figure 3, *a* and 4, *a* can be compared with the EKE spectra of a polycrystalline sample and a single-crystal film of MgF_2O_4 and of the single crystal of LiF_2O_4 [15], which coincide in all these cases (we have not found data on zinc ferrite magnetooptics in the literature). They contain four peaks in the region 2–4 eV: one very weak peak at 2.3 eV and three overlapping peaks at 2.6, 3.25 and 3.9 eV. The authors of the study [15] ascribed them to a single-ion transition $^6A_{1g}(^6S) \rightarrow {}^4E_g(^4G)$ and three two-exciton transitions: $2[^6A_{1g}(^6S) \rightarrow {}^4T_{1g}(^4G)]$, $[^6A_{1g}(^6S) \rightarrow {}^4T_{1g}(^4G) + {}^6A_{1g}(^6S) \rightarrow {}^4T_{2g}(^4G)]$ and $2[^6A_{1g}(^6S) \rightarrow {}^4T_{2g}(^4G)]$, respectively, where the energies of the transitions into the states T_{1g} and T_{2g} were 1.3 and 1.95 eV, respectively.

These types of the transitions can mainly contribute to a wide positive-sign structure in the zinc ferrite MCD spectrum when $x = 0.2$, which appears at 100 K (Figure 3, *a*) and to the same wide spectrum in the same region of the energies, but with a negative sign, in case of magnesium ferrite at $x = 0$, which is well observed already at 300 K. Positions of the specific features on the energy scale are quite similar for both the cases and for the cases represented in the study [15]: 2.5, 2.8, 3.08, 3.4 eV for Zn-ferrite and 2.3, 2.7, 2.98, 3.37, 3.88 eV for Mg-ferrite. In both the cases, a difference in the magnitude of the effects agrees with a difference in the value and the temperature dependence of magnetization. As some authors say (for example, as per the study [34,35]), the difference in the MCD sign can be related to a canting of magnetic sublattices in the MgF_2O_4 nanoparticles due to the influence of surface layers with broken bonds. This assumption is supported by similarity of the MCD spectrum (Figure 4, *a*) with a spectrum of the imaginary part of the off-diagonal component of the tensor g'' of the $FeBO_3$ weak ferromagnetic [36], which exhibited the specific features at the energies 2.8, 3.0 and 3.4 eV. Incorporation of Co destroys this structure and the contribution by the Fe^{3+} ions to the MCD signal quickly decreases.

In the studies dedicated to investigation of the magnetooptical effects in cobalt ferrite, the specific features in the EKE spectra or ε''_{xy} were observed near the energies 1.8 and 2.2 eV and identified as a spin-resolved transition between levels split in the crystal field (CF) in the tetrahedrally coordinated Co^{2+} ion: $^4A_2 \rightarrow {}^4T_2$ and as an intervalence charge transfer transition $[Co^{2+}]t_{2g} \rightarrow [Fe^{3+}]t_{2g}$, respectively [11,14,15,37]. Similarly, the specific features in the MCD spectrum of the cobalt ferrite nanoparticles were identified at the energies 1.81 and 2.25 eV in the study [38]. However, in the light of the Mössbauer effect data presented herein, the first of the discussed peaks at 1.75 eV can not be related to the transitions in the Co^{2+} ions localized in the tetrahedrons, since all the Co^{2+} ions occupy only the octahedral positions in our case. Generally speaking, it is considerably difficult to identify the CF electronic transitions in the Co^{2+} ions with the $3d^7$ electron configuration, since they occur at the close values of the light-wave energy both in the tetrahedral and the octahedral coordination [39]. Valuable information can be obtained from comparative study of the optical or magnetooptical spectra and the Mössbauer effect spectrum, which is realized in the present case. The respective comparison allows unambiguously relating the MCD peak near 1.75 eV to the spin-resolved transition $^4T_{1g} \rightarrow {}^4A_{2g}$ in the Co^{2+} ions in the octahedral positions. The absorption band caused by this transition was observed in the studies dedicated to compounds, in which the Co^{2+} ion entered the octahedral coordination only (see, for example, the studies [40,41]). This interpretation agrees with the fact that the intensity of the MCD signal at this energy increases in a proportion to the concentration of cobalt in the sample.

The positions of the peaks in the spectra EKE or MCD in the films or nanoparticles of cobalt ferrite at the higher light-wave energies and their identification differ in various authors. Zvyagin et al. [42] have studied the Kerr effect in a polar geometry and determined spectral dependences of the off-diagonal components of the permittivity tensor. They related the maximum in the spectrum of ε'' at 2.64 eV to the intersublattice transition (ISCT) between the Fe^{3+} ions that occupy the tetra- and octa-hedral positions $(Fe^{3+})t_2 \rightarrow [Fe^{3+}]t_{2g}$ and the specific feature at 3.41 eV to the intervalence transition (IVCT) between the bi- and trivalent ions in the identical positions $[Co^{2+}]t_{2g} \rightarrow [Fe^{3+}]e_g$. Fontijn et al. [11] also related an intense positive peak in the spectrum of ε''_{xy} in CoF_2O_4, which is observed by them at 2.6 eV, to the ISCT-transition $(Fe^{3+})t_2 \rightarrow [Fe^{3+}]t_{2g}$. The specific feature around 3.55 eV was related by them to the ISCT-transition $[Fe^{3+}]e_g \rightarrow (Fe^{3+})t_2$, too. This interpretation seems to be real, but some questions arise. Indeed, the specific feature near 2.6 eV is visible in the MCD spectra of all the presented samples (the difference of the MCD sign in case of magnesium ferrite was discussed above), i. e. it can be due to charge transfer between the Fe^{3+} ions in the different positions. The ratio between the concentrations of the Fe^{3+} ions in the octahedral and tetrahedral positions varies extremely slightly when incorporating cobalt, especially in case of Mg-ferrite (about 2%), while the intensity of the peak at 2.6 eV increases significantly. At the same time, the intensity of the negative peak around 3.5 eV decreases with the increase of the Co concentration, which contradicts both the models [11,42]. Probably, electronic transitions of another nature are also realized in the considered range of the spectrum and the observed MCD spectrum is caused by a number of overlapping peaks, including those that have different signs. The studies [14,15] have investigated the EKE in the CoF_2O_4 polycrystalline samples, which is represented by two wide positive-sign peaks centered at ~ 2.35 and 4.5 eV. The first of these peaks was associated by the authors of the study [14] with

the spin-resolved CF-transitions in the Co^{2+} ions in the octahedrons ${}^4T_{1g}({}^4F) \rightarrow {}^4A_{2g}$, ${}^4T_{1g}({}^4F) \rightarrow {}^4T_{1g}(P)$. Taking into account these transitions will result in an increase of the MCD signal with increase of the cobalt concentration, which is exactly observed in our case (compare Figure 3, *b* and *c* as well as Figure 4, *b* and *c*). However, the transition ${}^4T_{1g}({}^4F) \rightarrow {}^4A_{2g}$ is unambiguously associated with the negative peak at 1.75 eV. The second maximum in the EKE spectrum, which appears during cobalt incorporation, can result in a decrease of the MCD signal at the energies above 3.5 eV, which is shown in Figure 3, *c* and 4, *c*. Taking into account this transition does not allow a choice to be made between MCD mechanisms proposed in the studies [11,42]. Thus, it is quite difficult to interpret the MCD spectra of ferrites. A more detailed study of MCD in diluted cobalt ferrites now continues.

4. Conclusion

The nanoparticles $Zn_{1-x}Co_xFe_2O_4$ and $Mg_{1-x}Co_xFe_2O_4$ with $x = 0, 0.2$ and 0.4 were synthesized by the auto-combustion method using the citrate precursor. According to the X-ray diffraction data, the nanoparticles are cubic nanocrystals with the structure of cubic spinel of the space group *Fd-3m*. Despite using the identical technological conditions, distribution of the ions Co^{2+}, Fe^{3+}, Zn^{2+} and Mg^{2+} among the tetrahedral and octahedral positions in the crystal is sharply different, which plays a key role in forming the magnetic and magnetooptical properties of the synthesized nanoparticles. In case of Zn-ferrite the Zn^{2+} ions occupy mainly the tetrahedral positions (and only the tetrahedral positions during cobalt incorporation), while Fe^{3+} occupy predominantly the octahedral positions, and Co^{2+} is distributed approximately equally between both the types of the positions. A totally different pattern is observed for $Mg_{1-x}Co_xFe_2O_4$. The Mg^{2+} ions are mainly localized in the octahedrons, the Co^{2+} ions are localized only in the octahedrons, while the Fe^{3+} ions are distributed approximately equally between the octahedral and tetrahedral positions. Thus, distribution of the magnetic ions Co^{2+} and Fe^{3+} among the crystallographic positions in case of magnesium ferrite corresponds to their distribution in the ideal inverted ferrospinel.

The magnetic properties of the samples are also sharply different. When $x = 0$ the $Zn_{1-x}Co_xFe_2O_4$ nanoparticles demonstrate a purely paramagnetic behavior at the room temperature; during cobalt incorporation there are the field dependences of magnetization, which are typical for the magnetic-ordered state, wherein the values of magnetization are significant and the coercive forces are small. All the $Mg_{1-x}Co_xFe_2O_4$ samples are ferrimagnetic with high values of saturation magnetization and the coercive force.

The MCD signal in the ZnF_2O_4 nanoparticles at the room temperature is at a noise level, but at 100 K a noisy signal originates, thereby indicating formation of the magnetic-ordered phase according to the magnetic data and the low-temperature Mössbauer spectrum. The MCD spectra of the nanoparticles are highly changed when cobalt is incorporated and its concentration increases. In case of magnesium ferrite, the distinct spectra of MCD and FE are observed when $x = 0$ at the room temperature, and they differ from the zinc ferrite MCD spectrum. As the cobalt concentration increases, the shapes of the MCD spectra of both the systems become closer and closer to each other.

Special attention is paid to the MCD peak with the center at 1.75 eV. The wavelength that corresponds to the gravity center of this peak exactly coincides with the wavelength of radiation (710 nm) of some lasers, for example, ALP-710 nm produced by NKT Photonics (Denmark) and light-emitting diodes produced by many worldwide companies, for example, BMI SURPLUS Inc. (USA). It caused interest to using the studied nanoparticles in photonic devices. It has been analyzed to show that this peak is caused by the spin-allowed electronic transition in the crystal field in the octahedrally coordinated Co^{2+} ions.

Funding

The study was carried out within the framework of the research topic of the State Assignment of the Institute of Physics of the Siberian Branch of the Russian Academy of Sciences.

Conflict of interest

The authors declare that they have no conflict of interest.

References

[1] A.D. Buckingham, P.J. Stephens. Annu. Rev. Phys. Chem. **17**, 399 (1966).
[2] N.V. Starostin, P.P. Feofilov. UFN **97**, 621 (1969). (in Russian).
[3] P.N. Schatz, A.J. McCaffery. Q. Rev. Chem. Soc. **23**, *4*, 552 (1969).
[4] G.S. Krinchik, M.V. Chetkin. Sov. Phys. Uspekhi **12**, *3*, 307 (1969).
[5] A.K. Zvezdin, V.A. Kotov. Modern Magnetooptics and Magnetooptical Materials. Taylor & Francis Group, New York (1997). 404 p.
[6] T. Haider. Int. J. Electromag. Appl. **7**, *1*, 17 (2017).
[7] C. Rizal, H. Shimizu, J.R. Mejía-Salazar. Magnetochemistry **8**, *9*, 94 (2022).
[8] A.E. Rogachev, P.M. Vetoshko, N.A. Gusev, M.A. Kozhaev, A.R. Prokopov, V.V. Popov, D.V. Dodonov, A.G. Shumilov, A.N. Shaposhnikov, V.N. Berzhansky, A.K. Zvezdin, V.I. Belotelov. Appl. Phys. Lett. **109**, *16*, 162403 (2016).
[9] D. Vojna, O. Slezák, A. Lucianetti, T. Mocek. Appl. Sci. **9**, *15*, 3160 (2019).
[10] A. Abramovici, W.E. Althouse, R.W.P. Drever, Y. Gursel, S. Kawamura, F.J. Raab, D. Shoemaker, L. Sievers, R.E. Spero, K.S. Thorne, R.E. Vogt, R. Weiss, S.E. Whitcomb, M.E. Zucker. Sci. **256**, *5055*, 325 (1992).
[11] W.F.J. Fontijn, P.J. van der Zaag, R. Metselaar. J. Appl. Phys. **83**, *11*, 6765 (1998).

[12] W.F.J. Fontijn, P.J. van der Zaag, M.A.C. Devillers, V.A.M. Brabers, R. Metselaar. Phys. Rev. B **56**, *9*, 5432 (1997).
[13] W.F.J. Fontijn, P.J. van der Zaag, L.F. Feiner, R. Metselaar, M.A.C. Devillers. J. Appl. Phys. **85**, *8*, 5100 (1999).
[14] G.S. Krinchik, K.M. Mukimov, Sh.M. Sharipov, A.P. Khrebtov, E.M. Speranskaya. JETP **49**, *6*, 1074 (1979).
[15] G.S. Krinchik, A.P. Khrebtov, A.A. Askochenskii, E.M. Speranskaya, S.A. Belyaev. JETP **45**, *2*, 366 (1977).
[16] L. Stichauer, G. Gavoille, Z. Simsa. J. Appl. Phys. **79**, *7*, 3645 (1996).
[17] K.J. Kim, H.S. Lee, M.H. Lee, S.H. Lee. J. Appl. Phys. **91**, *12*, 9974 (2002).
[18] F.J. Kahn, P.S. Pershan, J.P. Remeika. Phys. Rev. **186**, *3*, 891 (1969).
[19] G.B. Scott, D.E. Lacklison, H.I. Ralph, J.L. Page. Phys. Rev. B **12**, *7*, 2562 (1975).
[20] P.E. Petrov, P.O. Kapralov, G.A. Knyazev, A.N. Kuzmichev, P.M. Vetoshko, Yu.M. Bunkov, V.I. Belotelov. Opt. Express **30**, *2*, 1737 (2022).
[21] M. Levy, O.V. Borovkova, C. Sheidler, B. Blasiola, D. Karki, F. Jomard, M.A. Kozhaev, E. Popova, N. Keller, V.I. Belotelov. Optica **6**, *5*, 642 (2019).
[22] A. Thakur, I. Edelman, D. Petrov, S. Ovchinnikov, P. Thakur, S. Zharkov, Y. Knyazev, A. Sukhachev. J. Mater. Res. **39**, *21*, 3029 (2024).
[23] G. Márquez, V. Sagredo, R. Guillén-Guillén, G. Attolini, F. Bolzoni. Revista Mexicana de Física **66**, *3*, 251 (2020).
[24] T.A.S. Ferreira, J.C. Waerenborgh, M.H.R.M. Mendonça, M.R. Nunes, F.M. Costa. Solid State Sci. **5**, *2*, 383 (2003).
[25] Bruker AXS TOPAS V4: General profile and structure analysis software for powder diffraction data. User's Manual. Bruker AXS, Karlsruhe, Germany (2008).
[26] R. Ivantsov, N. Evsevskaya, S. Saikova, E. Linok, G. Yurkin, I. Edelman. Mater. Sci. Eng. B **226**, 171 (2017).
[27] D. Chahar, S. Taneja, P. Thakur, A. Thakur. J. Alloys Compd **843**, 155681 (2020).
[28] O.S. Ivanova, I.S. Edelman, S.G. Ovchinnikov, A. Thakur, P. Thakur, A.L. Sukhachev, Y.V. Knyazev, R.D. Ivantsov, M.S. Molokeev. JETP Lett. **119**, *2*, 104 (2024).
[29] S. Sarmah, K.P. Patra, P.K. Maji, S. Ravi, T. Bora. Ceram. Int. **49**, —it 1, 1444 (2023).
[30] M. Al-Maashani, A.M. Gismelseed, K.A.M. Khalaf, A.A. Yousif, A.D. Al-Rawas, H.M. Widatallah, M.E. Elzain. Hyperfine Interactions **239**, *1*, 15 (2018).
[31] H.B. Desai, A. Kumar, A.R. Tanna. Eur. Chem. Bull. **10**, *3*, 186 (2021).
[32] W.S. Mohamed, M. Alzaid, M.S.M. Abdelbaky, Z. Amghouz, S. García-Granda, A.M. Abu-Dief. Nanomater. **9**, *11*, 1602 (2019).
[33] S.S. Jadhav, S.E. Shirsath, B.G. Toksha, S.M. Patange, S.J. Shukla, K.M. Jadhav. Int. J. Modern Phys. B **23**, *30*, 5629 (2009).
[34] L.M. Corliss, J M. Hastings, F.G. Brockman. Phys. Rev. **90**, *6*, 1013 (1953).
[35] V. Šepelák, A. Feldhoff, P. Heitjans, F. Krumeich, D. Menzel, F.J. Litterst, I. Bergmann, K.D. Becker. Chem. Mater. **18**, *13*, 3057 (2006).
[36] A.V. Malakhovsky, I.S. Edelman. Physica Status Solidi B **74**, *2*, K145 (1976).
[37] W.D. Martens, W.L. Peeters, H.M. Noort, M. Erman. J. Phys. Chem. Solids **46**, *4*, 411 (1985).
[38] B.S. Holinsworth, N.C. Harms, S. Fan, D. Mazumdar, A. Gupta, S.A. McGill, J.L. Musfeldt. APL Mater. **6**, *6*, 066110 (2018).
[39] D.T. Sviridov, R.K. Sviridova, Yu.F. Smirnov. Opticheskie spektry ionov perekhodnykh metallov v kristallakh. Nauka, M. (1976). 266 s. (in Russian).
[40] K. Ravindranadh, K.D.V. Prasad, M.C. Rao. AIMS Mater. Sci. **3**, *3*, 796 (2016).
[41] M.N. Taran, G.R. Rossman. Am. Mineral. **86**, *7*, 889 (2001).
[42] V. Zviagin, P. Richter, T. B"ontgen, M. Lorenz, M. Ziese, D.R.T. Zahn, G. Salvan, M. Grundmann, R. Schmidt-Grund. Physica Status Solidi B **253**, *3*, 429 (2016).

Translated by M.Shevelev